Magnetic-sublevel cross sections for excitation of the $n\ ^1P$ levels of helium by electron impact

George Csanak and David C. Cartwright
University of California, Los Alamos National Laboratory, Los Alamos, New Mexico 87545

Sandor Trajmar
Jet Propulsion Laboratory, California Institute of Technology, Pasadena, California 91109
(Received 26 December 1990)

First-order many-body theory has been used to calculate collision-frame magnetic-sublevel differential cross sections for electron-impact excitation of the $n\ ^1P$ ($n=2,3,4,5,6$) levels of helium for electrons with incident energy in the 25–500-eV range. By combining results from electron-impact differential-cross-section measurements and electron-photon coincidence measurements, experimental magnetic-sublevel cross sections have also been derived for the excitation of the $2\ ^1P$ and $3\ ^1P$ levels. The theory predicts a pronounced minimum for the $M=0$ magnetic-sublevel differential cross section for incident electron energies around 30 eV. Our theoretical results are compared to the experimental data and some other theoretical results.

PACS number(s): 34.80.Dp

I. INTRODUCTION

Electron-scattering measurements have historically been concerned with the determination of differential cross sections (DCS's) or integral cross sections (ICS's) representing the usual statistical averages over unresolved states (sum-over-final and average-over-initial states). This averaging and summation includes the magnetic-sublevel structure and hyperfine, or otherwise experimentally unresolved, sublevels of the initial and final levels of the target. With the development of electron-photon coincidence (EPC) techniques [1,2], it is now possible to obtain magnetic-sublevel excitation cross sections for the electron-impact excitation of atomic systems. Results from electron-photon coincidence measurements are usually presented in the form of various electron-impact coherence parameters (EICP) and extensive reviews on this subject were published recently by Andersen, Gallagher, and Hertel [3] and by Slevin and Chwirot [4]. While the terminology of the EICP's is somewhat complex, and can be confusing for the average collision physicist, it is easy to understand the concept of magnetic-sublevel DCS's. It is the purpose of the present work to point out that information from EPC experiments and from conventional DCS measurements can be used to obtain magnetic-sublevel DCS's. In the case of a $^1S\rightarrow{}^1P$ excitation, which is the subject of the present paper, the λ parameter [1–4] represents the ratio of the ^1P ($M=0$) magnetic-sublevel DCS to the magnetic-sublevel summed DCS.

We call the collection of magnetic sublevels for a specific n the $n\ ^{2S+1}L$ "level" and reserve the term "state" for identifying the individual magnetic sublevels and identify the experimentally determined magnetic sublevel DCS with an M-value subscript.

The notation $d\sigma/d\Omega$ for the theoretical differential cross section, and DCS for the experimentally obtained quantity, are used interchangeably here because they are equivalent to within experimental error. DCS is also used for the abbreviation of "differential cross section." Correspondingly, the symbols σ for the theoretical and Q for the experimental integral cross sections are used interchangeably, and σ_M^c refers to the "theoretical ICS in the collision frame for the excitation of the magnetic sublevel M."

The axis of quantization, the Z axis of the coordinate system, was chosen along the direction of the incident electron beam, and the (X,Z) plane coincides with the collision plane. This latter coordinate system is usually referred to as the "collision frame" and is the frame used to obtain the results reported in this paper. The λ parameter, combined with available DCS data, can yield, therefore, the individual collision-frame magnetic-sublevel DCS's. This latter approach was utilized by Chutjian and Srivastava [5] for the excitation of the $2\ ^1P$ level of helium at 60- and 80-eV impact energies and by Chutjian [6] for excitation of the $3\ ^1P$ level at 80 and 100 eV, whereas Hummer and Burns [7] directly obtained from an EPC experiment the $M=0$ magnetic-sublevel DCS for the excitation of the $3\ ^1P$ level at 70 eV.

In this paper we utilize the λ parameters and the DCS's, which recently became available from laboratory measurements, to deduce the corresponding collision-frame magnetic-sublevel DCS's. We also present differential and integral cross-section results obtained using first-order many-body theory [8] (FOMBT). The experimental and theoretical results are compared to each other, and some general conclusions

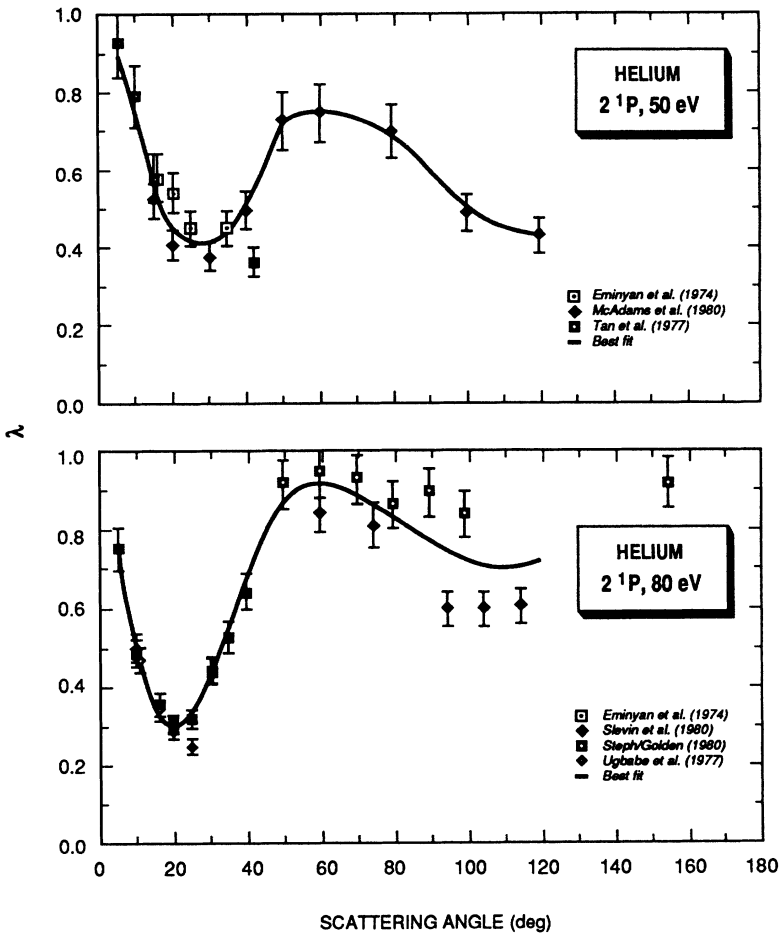

FIG. 1. λ values available for the $2\,^1P$ level at 50 eV (upper panel) and 80 eV (lower panel). The experimental results shown are (a) at 50 eV, that of Eminyan *et al.* (Ref. [9]), McAdams *et al.* (Ref. [10]), and Tan *et al.* (Ref. [11]) and (b) at 80 eV that of Eminyan *et al.* (Ref. [9]), Slevin *et al.* (Ref. [12]), Steph and Golden (Ref. [13]), and Ugbabe *et al.* (Ref. [14]). The smooth line drawn through these points denotes the values used in this paper for each incident electron energy.

TABLE I. Summary of impact energies and angular ranges for which magnetic-sublevel DCS's were obtained from experimental data and sources of DCS and EICP data.

Level	E (eV)	Angular range (deg)	References DCS	λ
$2\,^1P$	26.5	7.5–70	[16]	[17,18]
	30	10–130	[19]	[17,10,20]
	40	10–110	[21]	[20,9]
	50	5–120	[19]	[10,9,11,22]
	60	10–120	[5][a]	[9,12,22]
	80	5–120	[5][a]	[9,12,13] [14,22]
	100	5–40	[19]	[9,13]
	200	7.5–35	[23]	[9,13]
	500	7.5–20	[23]	[13]
$3\,^1P$	50	5–90	[19]	[22,24]
	70	10–50	[7]	[7]
	80	10–110	[6][b]	[22,24,25,26]
	100	10–30	[6][b],[19]	[24]

[a]DCS values of Ref. [5] were renormalized (see text).
[b]DCS values of Ref. [6] were renormalized (see text).

TABLE II. Summary of experimental $2\,^1P$ differential cross sections (10^{-18} cm^2 sr^{-1}), λ values, and derived magnetic-sublevel differential cross sections (10^{-18} cm^2 sr^{-1}), last two columns.

				DCS	
E (eV)	θ (deg)	DCS (all M)	λ	$M=0$	$M=1$
26.5	7.5	0.39	0.97	0.38	0.005
	10	0.45	0.95	0.43	0.010
	13	0.73	0.94	0.69	0.020
	20	1.51	0.89	1.34	0.085
	30	1.51	0.82	1.24	0.135
	40	0.90	0.73	0.66	0.120
	50	0.43	0.63	0.27	0.140
	60	0.22	0.52	0.11	0.055
	70	0.10	0.43	0.043	0.030
30	10	5.05	0.93	4.70	0.175
	15	3.73	0.87	3.25	0.24
	20	2.77	0.81	2.24	0.265
	30	1.30	0.70	0.91	0.195
	40	0.46	0.59	0.27	0.095
	50	0.26	0.50	0.13	0.065
	60	0.15	0.44	0.066	0.043
	70	0.12	0.44	0.053	0.034
	80	0.10	0.45	0.054	0.033
	90	0.097	0.43	0.042	0.028
	100	0.091	0.37	0.034	0.029
	110	0.073	0.30	0.022	0.026
	120	0.075	0.26	0.020	0.028
	130	0.099	0.25	0.025	0.037
40	10	10.7	0.84	8.99	0.885
	20	4.88	0.63	3.07	0.905
	30	1.71	0.49	0.84	0.435
	40	0.63	0.49	0.31	0.160
	50	0.30	0.56	0.17	0.065
	60	0.19	0.63	0.12	0.035
	70	0.15	0.69	0.10	0.025
	80	0.12	0.73	0.090	0.015
	90	0.10	0.74	0.075	0.013
	100	0.098	0.73	0.071	0.014
	110	0.080	0.70	0.056	0.012
50	5	28.9	0.90	26.0	1.45
	10	17.5	0.75	13.1	2.20
	15	10.5	0.56	5.99	2.26
	20	6.42	0.45	2.89	1.77
	30	2.16	0.41	0.89	0.635
	40	0.80	0.50	0.40	0.200
	50	0.38	0.72	0.27	0.055
	60	0.27	0.75	0.20	0.035
	70	0.20	0.73	0.15	0.025
	80	0.16	0.69	0.11	0.025
	90	0.12	0.60	0.072	0.024
	100	0.096	0.50	0.048	0.024
	110	0.077	0.45	0.035	0.021
	120	0.069	0.43	0.030	0.020
60	10	23.0	0.60	13.8	4.60
	15	11.0	0.48	5.28	2.86
	20	5.5	0.40	2.2	1.65
	30	1.3	0.40	0.52	0.39
	40	0.36	0.64	0.23	0.065
	50	0.19	0.83	0.16	0.016

TABLE II. (*Continued*).

E (eV)	θ (deg)	DCS (all M)	λ	DCS $M=0$	DCS $M=1$
	60	0.12	0.88	0.106	0.007
	75	0.083	0.81	0.067	0.008
	80	0.066	0.75	0.050	0.008
	90	0.055	0.65	0.036	0.009
	105	0.045	0.60	0.027	0.009
	120	0.034	0.53	0.018	0.008
80	5	52.0	0.75	39.00	6.50
	8	36.0	0.55	19.80	8.10
	10	26.0	0.49	12.74	6.63
	15	10.5	0.36	3.78	3.36
	20	4.3	0.30	1.29	1.51
	25	1.9	0.32	0.61	0.65
	30	0.77	0.44	0.34	0.22
	35	0.41	0.53	0.22	0.096
	40	0.23	0.66	0.15	0.039
	50	0.12	0.87	0.10	0.001
	60	0.080	0.91	0.073	0.0036
	75	0.051	0.86	0.044	0.0036
	80	0.042	0.83	0.035	0.0036
	90	0.034	0.77	0.026	0.0039
	105	0.023	0.70	0.016	0.0035
	120	0.019	0.72	0.014	0.0025
100	5	78.9	0.66	52.1	13.4
	10	29.8	0.37	11.0	14.4
	15	10.9	0.28	3.05	3.93
	20	3.86	0.25	0.97	1.40
	30	0.53	0.45	0.24	0.145
	40	0.17	0.74	0.13	0.020
200	7.5	38.4	0.27	10.4	14.00
	10	17.2	0.20	3.44	6.90
	15	3.56	0.14	0.50	1.53
	20	0.81	0.20	0.16	0.325
	25	0.23	0.42	0.097	0.065
	30	0.087	0.63	0.055	0.017
	35	0.052	0.80	0.042	0.005
500	7.5	10.86	0.125	1.36	4.75
	10	3.24	0.090	0.29	1.48
	15	0.32	0.14	0.045	0.24
	20	0.040	(0.29)	0.012	0.014

are drawn concerning the status of the theory based on these comparisons.

II. CROSS SECTIONS OBTAINED FROM EXPERIMENTAL DATA

A. Procedure

The following procedure was employed to obtain experimentally "measured" magnetic-sublevel DCS's. All measured λ values available for helium $n\,^1P$ ($n=2,3$) excitation were collected and plotted as a function of scattering angle (θ) for each impact energy (E), as shown in Fig. 1. A smooth curve was then drawn through the data points (Fig. 1) and the λ values at various intermediate-scattering angles were interpolated from these curves. The literature was also surveyed for all $n\,^1P$ ($n=2,3$) excitation DCS's, and some of the older data derived from inelastic- to elastic-scattering intensity ratios were renormalized using the more recent elastic-scattering DCS data [15]. Multiplication of the appropriate λ and the DCS values yields the collision DCS

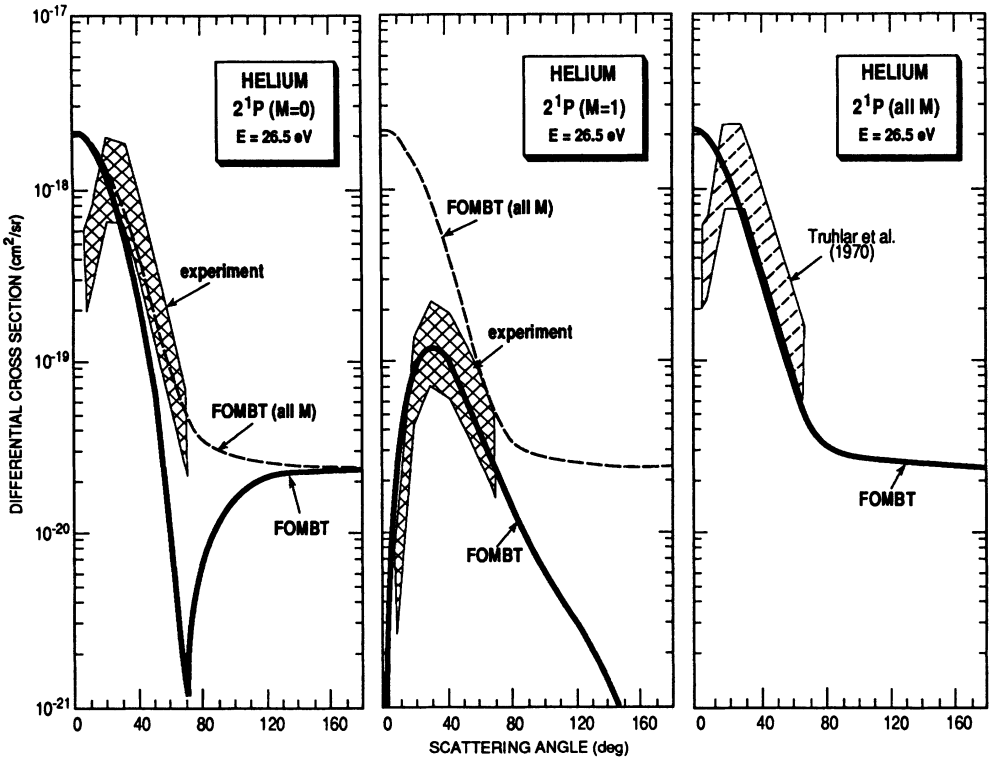

FIG. 2. Magnetic-sublevel DCS's (left two panels) and magnetic-sublevel summed DCS (right panel) for the electron-impact excitation of the $2\,^1P$ state of helium at $E=26.5$ eV incident electron energy. The "experimental" values for collision DCS's for $M=0$ (left panel) and $M=1$ (middle panel) were obtained as described in the text. The experimental DCS data in the right panel are from Truhlar *et al.* [16]. The results of our calculations are indicated by FOMBT, and the magnetic-sublevel summed DCS obtained from our FOMBT calculation is shown as a dashed line in all three panels to provide a reference for comparisons.

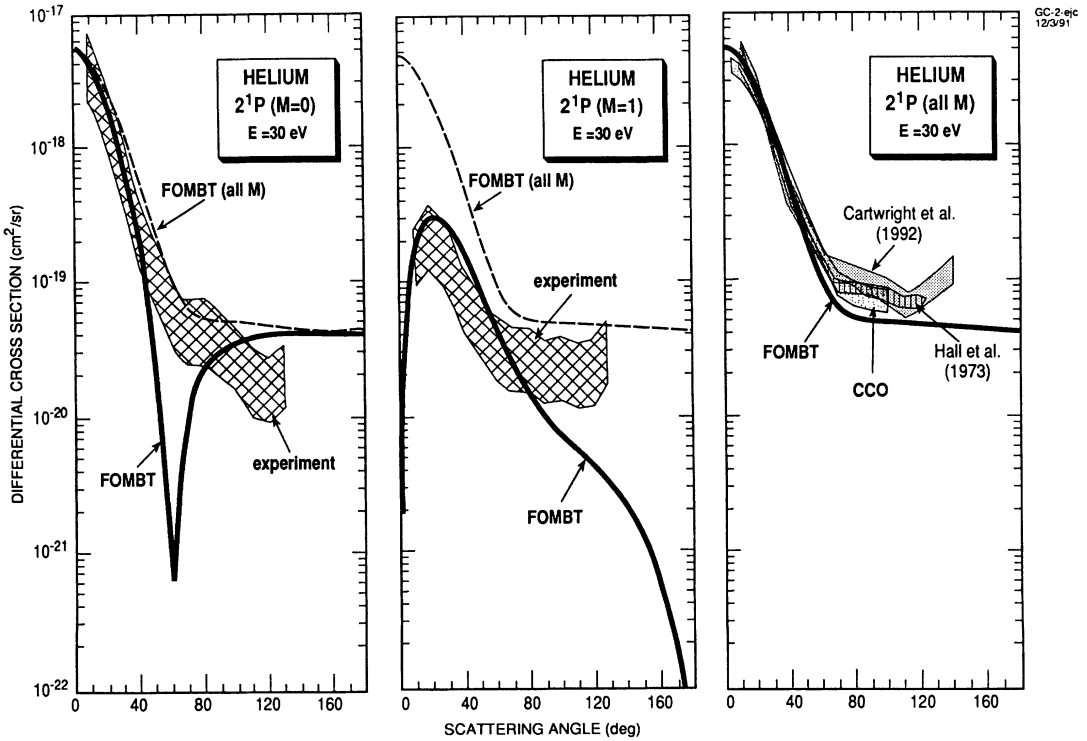

FIG. 3. Same as Fig. 2 except for $E=30$ eV incident electron energy. The experimental DCS data used are from Cartwright *et al.* [19] and from Hall *et al.* [21] (shown in right panel). The ten-channel optical potential close-coupling (CCO) results of Brunger *et al.* [27] for the DCS are also shown.

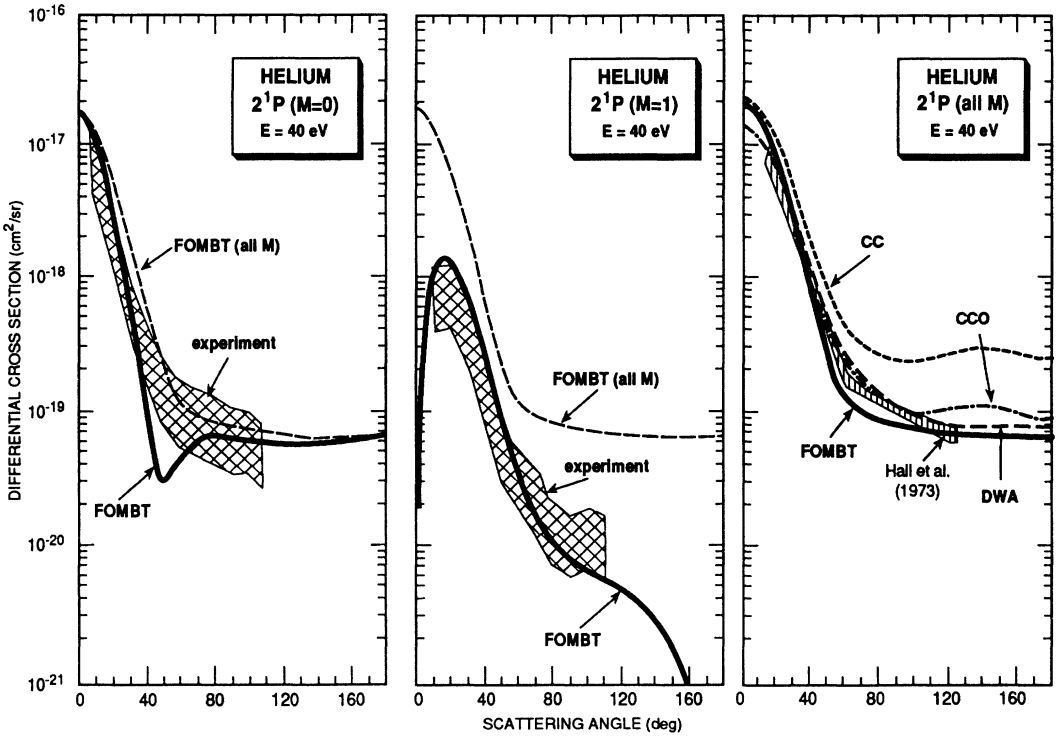

FIG. 4. Same as Fig. 2 except for $E = 40$ eV incident electron energy. The experimental DCS data used are from Hall *et al.* [21] (shown in right panel). The distorted-wave-approximation (DWA) results of Madison and co-workers [28], the five-state close-coupling (five-state CC) results of Bhadra, Callaway, and Henry [29] and the ten-channel optical potential close-coupling (CCO) results of Brunger *et al.* [27] are also shown in the right panel for comparison.

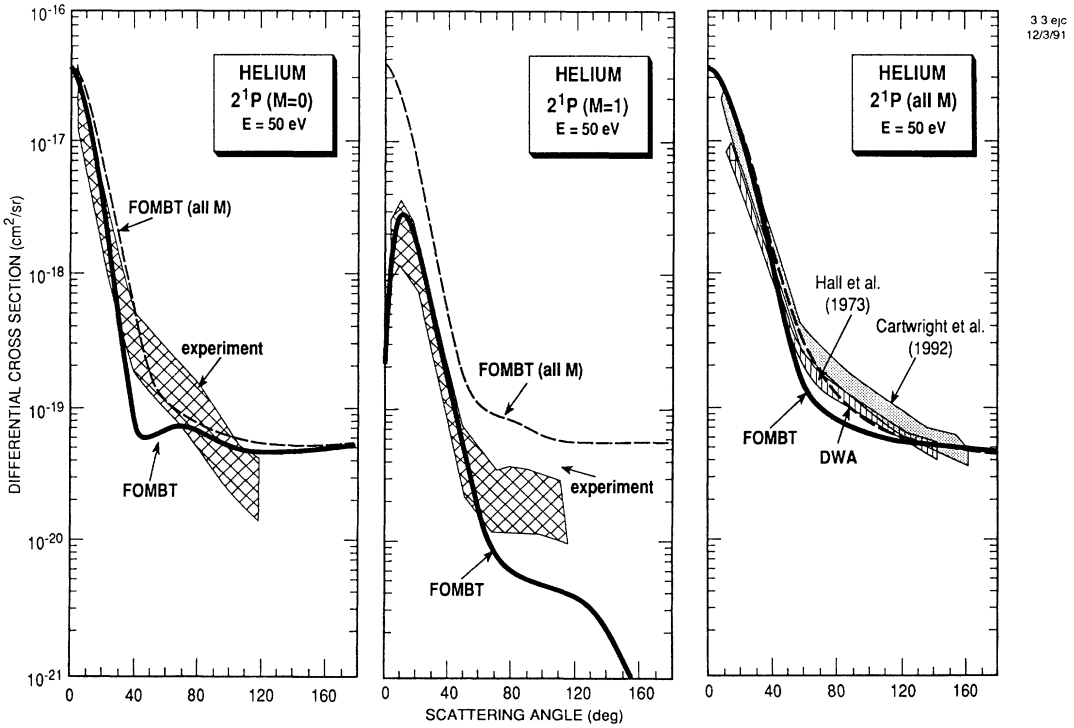

FIG. 5. Same as Fig. 3 except for $E = 50$ eV incident electron energy. The experimental DCS data used are from Hall *et al.* [21] and from Cartwright *et al.* [19] (shown in the right panel). The DWA results of Madison and co-workers [28] are also shown in the right panel for comparison.

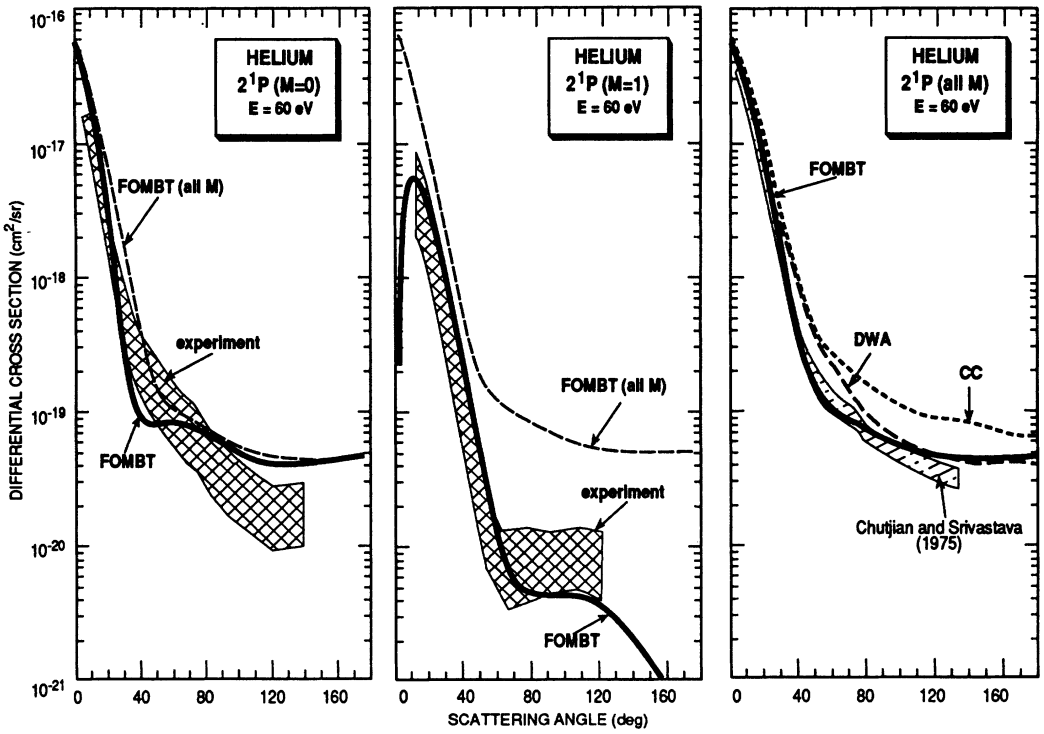

FIG. 6. Same as Fig. 2 except for $E = 60$ eV incident electron energy. The experimental DCS data used are from Chutjian and Srivastava [5] (shown in the right panel). The DWA results of Madison and co-workers [28] and the five-state CC results of Bhadra, Callaway, and Henry [29] are also shown in the right panel, as well as earlier FOMBT results of Thomas *et al.* [30] for comparison.

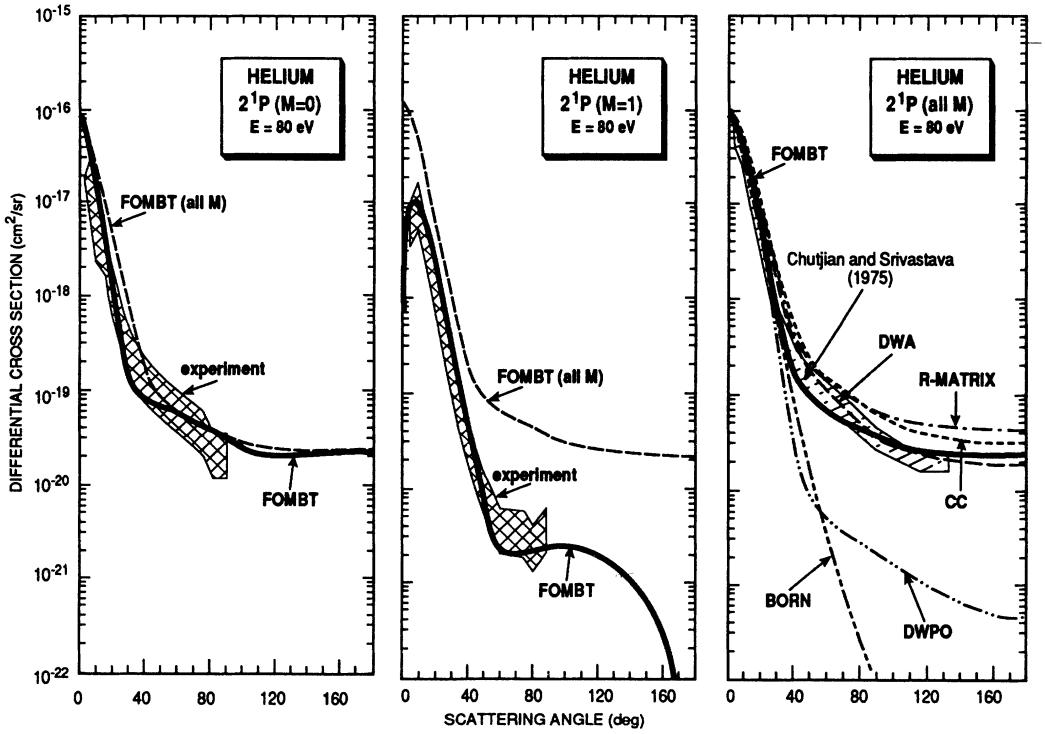

FIG. 7. Same as Fig. 2 except for $E = 80$ eV incident electron energy. The experimental DCS data used are from Chutjian and Srivastava [5] (shown on the right panel). The DWA results of Madison and co-workers [28], the five-state CC results of Bhadra, Callaway, and Henry [29], the five-state R-matrix (R-MATRIX) results of Fon, Berrington, and Kingston [31], the distorted-wave polarized orbital (DWPO) results of Scott and McDowell [32], and the present Born approximation (BORN) results are also shown in the right panel for comparison.

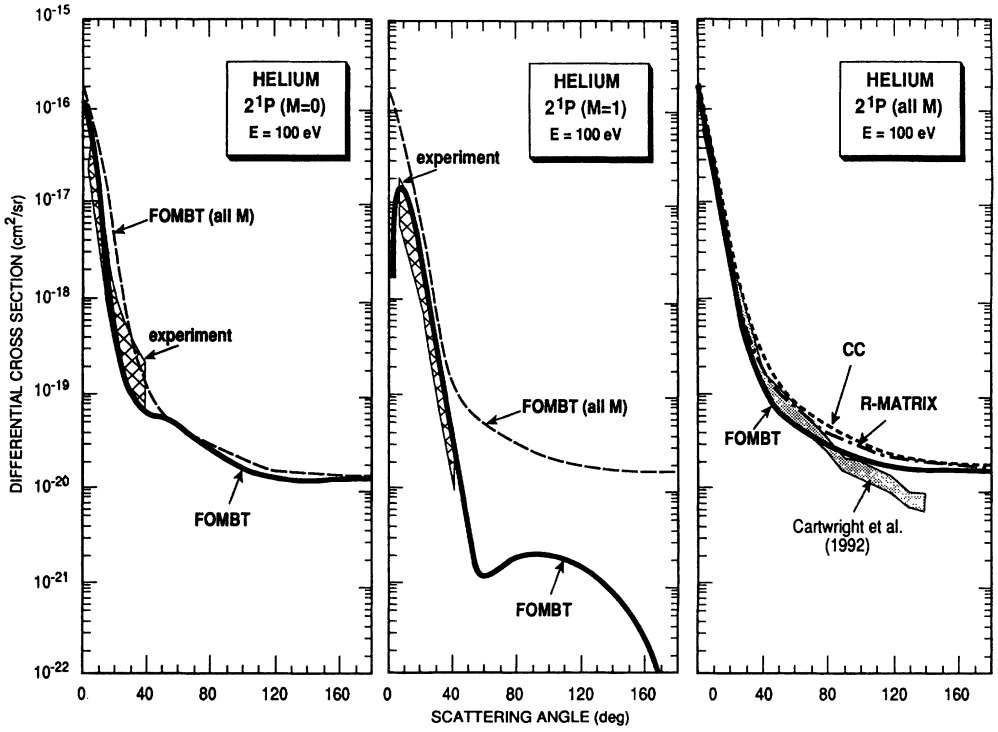

FIG. 8. Same as Fig. 2 except for $E = 100$ eV incident electron energy. The experimental DCS data used are from Cartwright *et al.* [19] (shown in the right panel). The five-state CC results of Bhadra, Callaway, and Henry [29] and the five-state R-matrix (R-MATRIX) results of Fon, Berrington, and Kingston [31] are also shown.

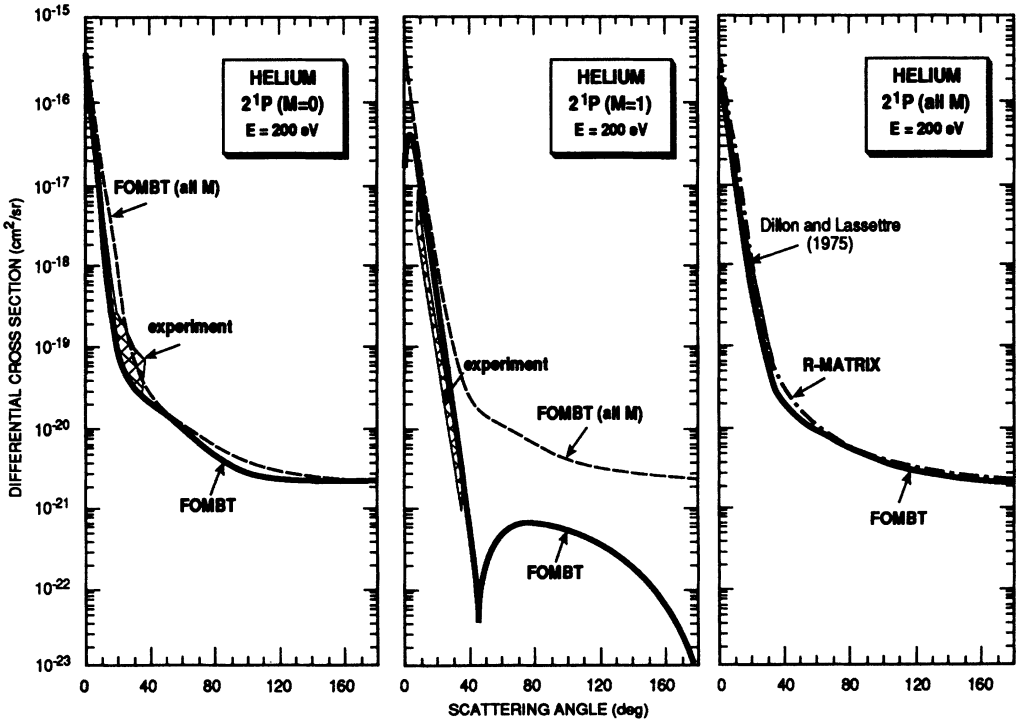

FIG. 9. Same as Fig. 2 except for $E = 200$ eV incident electron energy. The experimental DCS data used are from Dillon and Lassettre [23] (shown in the right panel). The five-state R-MATRIX results of Fon, Berrington, and Kingston [31] are also shown.

TABLE III. Summary of experimental $3\,^1P$ differential cross sections (10^{-18} cm^2 sr^{-1}), λ values, and derived magnetic-sublevel differential cross sections (10^{-18} cm^2 sr^{-1}), last two columns.

E (eV)	θ (deg)	DCS (all M)	λ	DCS $M=0$	DCS $M=1$
50	5	5.55	(0.84)	(4.78)	(0.46)
	10	3.50	(0.70)	(2.52)	(0.54)
	15	2.36	0.57	1.39	0.53
	20	1.50	0.51	0.80	0.39
	30	0.57	0.50	0.31	0.15
	40	0.20	0.60	0.14	0.046
	50	0.084	0.74	0.074	0.013
	60	0.065	0.81	0.062	0.0075
	70	0.052	0.77	0.045	0.0070
	80	0.042	0.71	0.035	0.0070
	90	0.034	(0.69)	(0.026)	(0.0060)
70[a]	10			6.0	
	15			3.7	
	20			2.2	
	25			1.3	
	30			0.63	
	35			0.30	
	40			0.22	
	50			0.13	
80[b]	10	5.8	0.51	2.96	1.42
	15	2.7	0.38	1.03	0.84
	20	1.1	0.34	0.37	0.37
	25	0.46	0.33	0.15	0.16
	30	0.21	0.40	0.084	0.065
	40	0.073	0.56	0.041	0.032
	50	0.047	0.77	0.036	0.0055
	60	0.031	0.85	0.026	0.0025
	90	0.013	0.53	0.0069	0.0031
	110	0.0071	0.64	0.0045	0.0013
80[c]	10	6.2	0.51	3.2	1.5
	15	2.8	0.38	1.1	0.85
	20	1.1	0.34	0.37	0.73
	25	0.47	0.33	0.16	0.31
	30	0.24	0.40	0.096	0.144
100[b]	10	7.32	0.45	3.29	2.01
	15	2.93	0.28	0.82	1.06
	20	1.12	0.31	0.35	0.39
	25	0.39	0.39	0.15	0.12
	30	0.16	0.58	0.093	0.067
100[c]	10	8.2	0.45	3.7	2.25
	15	3.3	0.28	0.92	1.20
	20	1.2	0.31	0.37	0.42
	25	0.4	0.39	0.16	0.12
	30	0.15	0.58	0.087	0.032

[a]Relative data (Ref. [7]) normalized to FOMBT result at 10° scattering angle.
[b]Renormalized data of Ref. [6]. (See text).
[c]Original values published by Chutjian (Ref. [6]). Numbers in parentheses were obtained by extrapolation.

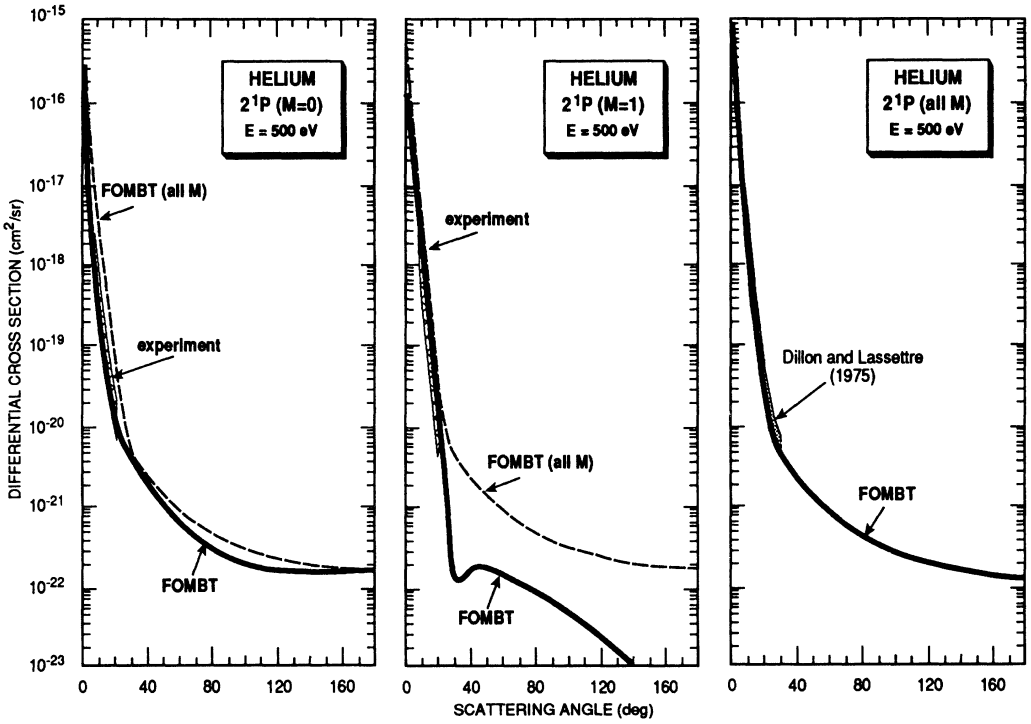

FIG. 10. Same as Fig. 2 except for $E = 500$ eV incident electron energy. The experimental DCS data used are from Dillon and Lassettre [23] (shown in the right panel).

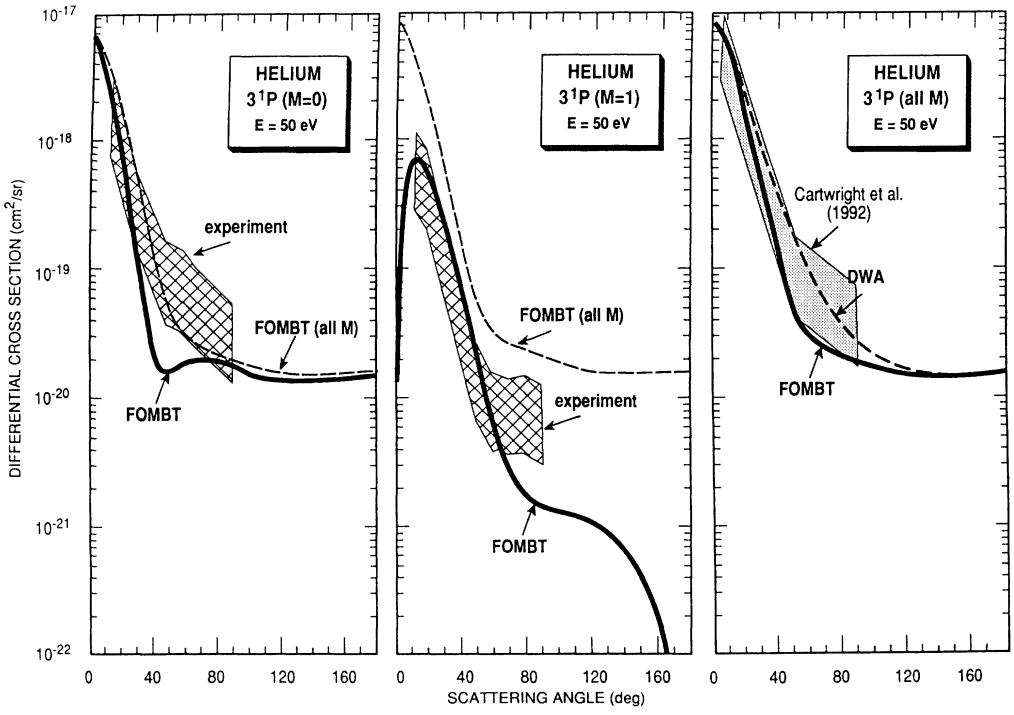

FIG. 11. Same as Fig. 2 except for magnetic-sublevel DCS's (left two panels) and magnetic-sublevel summed DCS (right panel) for the electron-impact excitation of the $3\,^1P$ state of helium at $E = 50$ eV incident electron energy. The experimental DCS data used (shown in the right panel) are from Cartwright *et al.* [19]. As with the previous figures, the summed magnetic-sublevel DCS has been included in the left and center panels as the dashed curve to enable comparison with the magnetic-sublevel DCS.

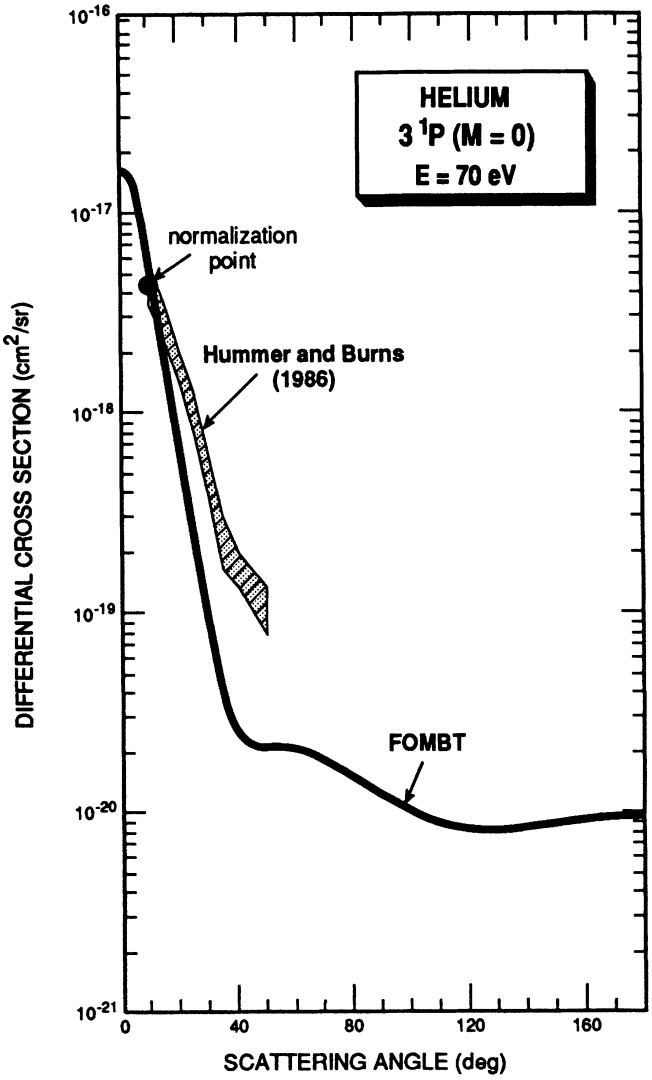

FIG. 12. Comparison of FOMBT results for the DCS ($M=0$) with the experimental data of Hummer and Burns [7] for $E=70$ eV incident electron energy. The relative experimental DCS ($M=0$) results were normalized to our FOMBT results at the smallest experimental scattering angle ($\theta=10°$).

($M=0$); subtraction of this quantity from the DCS and division of the quantity by 2 yields the DCS's for which $M=1$ and -1 are equal.

The energy and angular regions for generating measured magnetic-sublevel cross sections are limited to those for which *both* the λ parameters and DCS's are available from experiments. In Table I we summarize these regions of overlap and the associated references. The λ values and magnetic-sublevel DCS's derived by our procedure for the $2\,^1P$ level are given in Table II and compared with FOMBT results in Figs. 2–10. For excitation of the $3\,^1P$ level, the data available for both the λ parameter and the DCS, which are very meager, are summarized in Table III and compared with FOMBT results in Figs. 11–14. No data are available for $n \geq 4$ levels.

It is not possible to give precise error limits for the "experimental" magnetic sublevel DCS's because the uncertainties associated with the λ parameters are not well established. In some cases only one-standard-deviation error is given, which reflects only the fitting of the experimental data to appropriate analytical expressions for extracting the λ parameters, and other experimental errors are neglected. In some cases the experimental error limits quoted by various experimentalists for the same λ do not overlap. After examining the reported data, the procedures applied to obtain them, and the scatter in the available data points, we estimate that the λ values are generally known to about $\pm 20\%$ and the DCS values to about $\pm 15\%$ to 20%. Taking the square root of the squares of the two contributing uncertainties, we estimate that the magnetic-sublevel DCS's presented here from various measurements are accurate to about $\pm 25\%$. At small scattering angles for most impact energies, the λ parameters are known to be better than $\pm 20\%$, but for these cases the DCS values are subject to larger errors. At high scattering angles λ values are scarce and subject

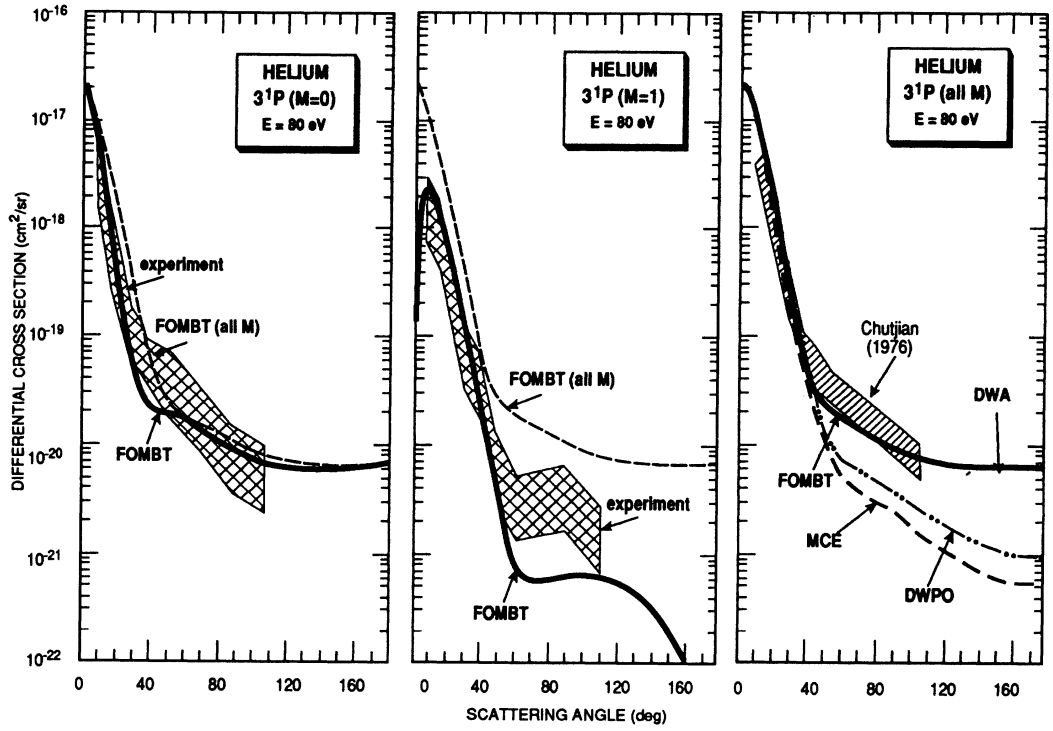

FIG. 13. Same as Fig. 11 except for $E = 80$ eV incident electron energy. The experimental DCS data used (shown in the right panel) are from Chutjian [6]. The DWA results of Madison and co-workers [28], the DWPO results of Scott and McDowell [32], and the multichannel eikonal theory (MCE) results of Flannery and McCann [33] are also shown (in the right panel).

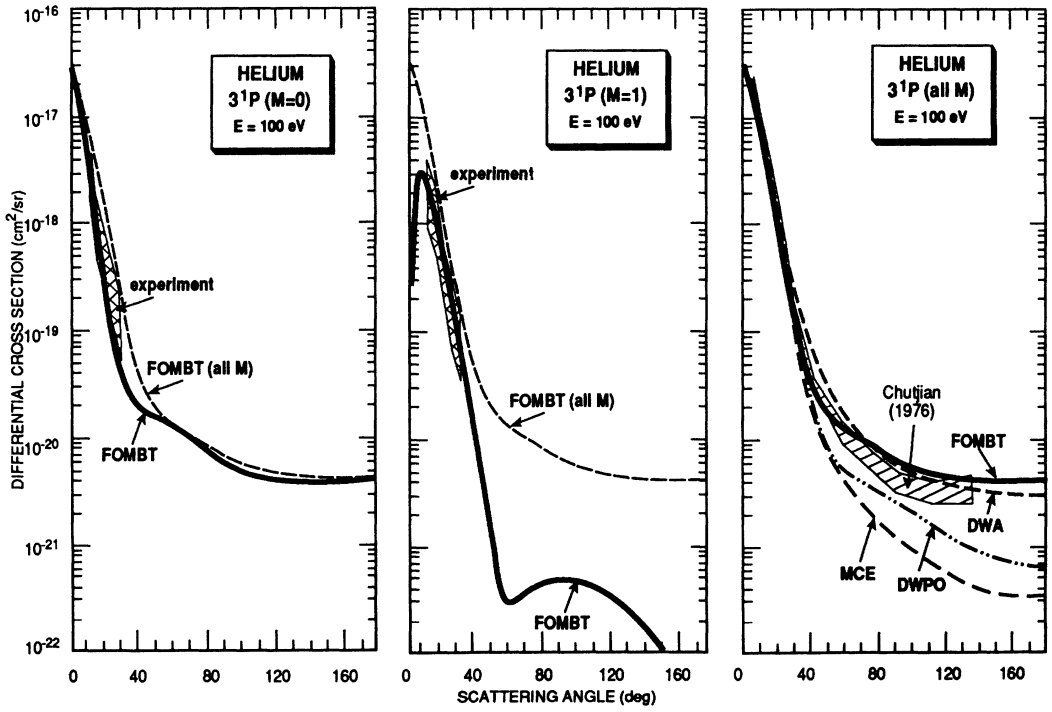

FIG. 14. Same as Fig. 11 except for $E = 100$ eV incident electron energy. The experimental DCS data used (shown in the right panel) are from Chutjian [6]. DWA results of Madison and co-workers [28], DWPO results of Scott and McDowell [32], and MCE theory results of Flannery and McCann [33] are also shown.

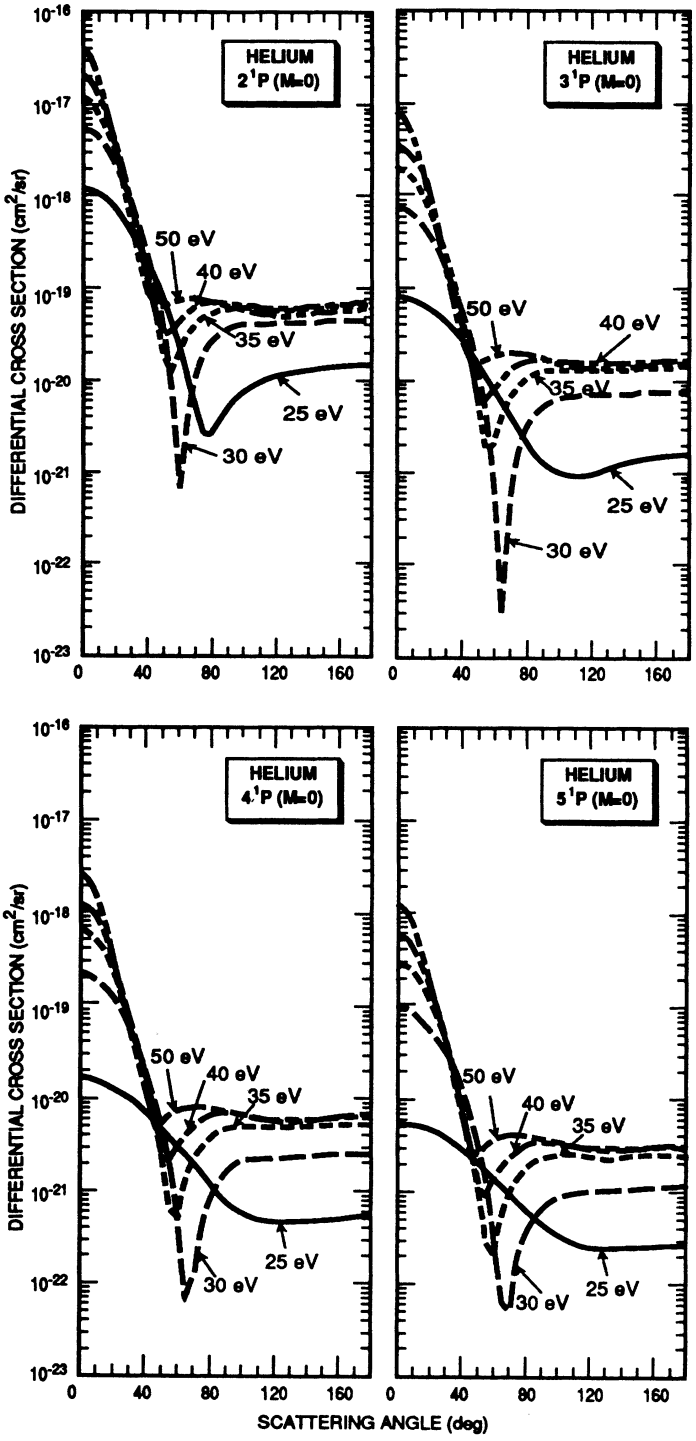

FIG. 15. FOMBT results for the DCS ($M=0$) in the incident electron range of 25 eV $\leq E \leq$ 50 eV for (a) $2\,^1P$ ($M=0$) excitation (upper left); (b) $3\,^1P$ ($M=0$) excitation (upper right). (c) $4\,^1P$ ($M=0$) excitation (lower left); (d) $5\,^1P$ ($M=0$) excitation (lower right).

to larger than ±20% uncertainties, but the DCS's are more accurately known.

B. Excitation of the $2\,^1P$ level

Following the procedure outlined above, the magnetic-sublevel cross sections for excitation of the $2\,^1P$ level given in Table II and shown in Figs. 2–10 were derived at impact energies ranging from 26.5 to 500 eV.

(a) At 26.5 eV the λ parameters were obtained from the measurements of van Linden van den Heuvell, van Eck, and Heideman [17] and Crowe and Nogueira [18]. The DCS's were taken from Truhlar *et al.* [16], but those

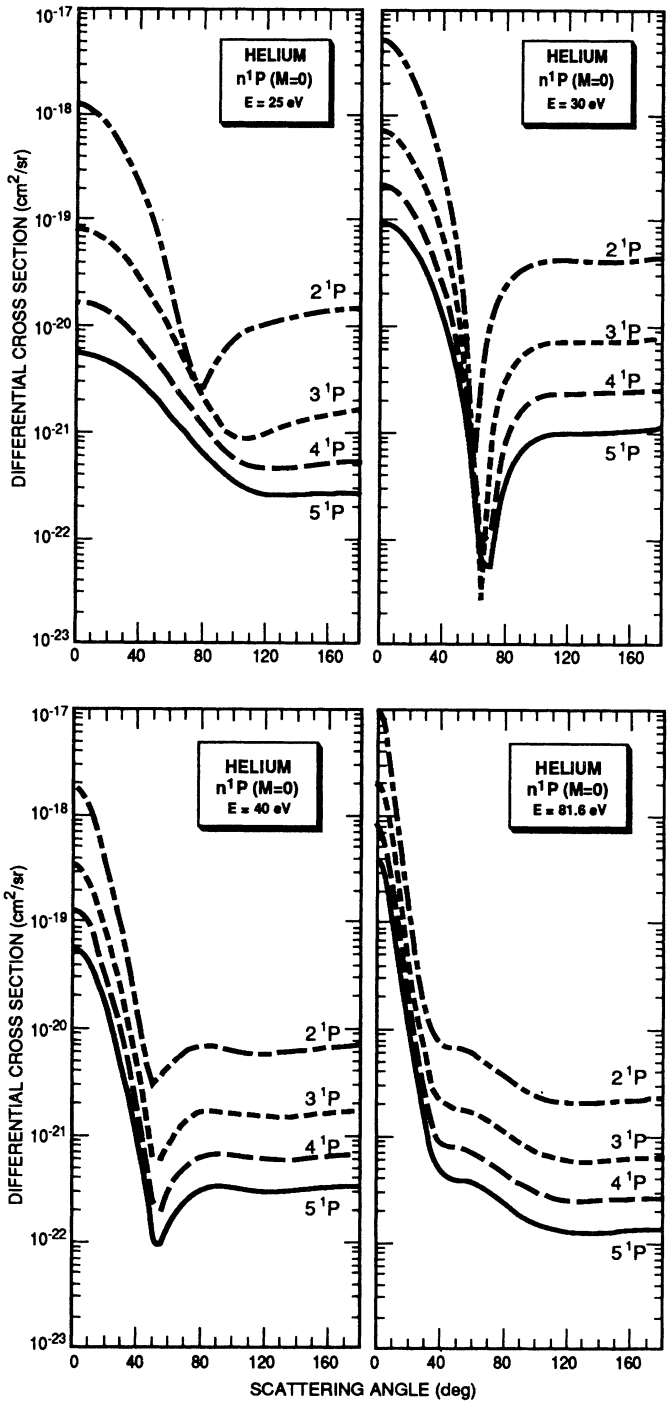

FIG. 16. FOMBT results for the DCS ($M=0$) for excitation of the $n\,^1P$ ($n=2$–5) states of helium. (a) 25-eV incident electron energy (upper left); (b) 30-eV incident electron energy (upper right); (c) 40-eV incident electron energy (lower left); (d) 81.6-eV incident electron energy (lower right).

values were multiplied by a factor of 2 because the integral cross sections used by Truhlar *et al.* [16] for normalization (derived by Jobe and St. John [34] from optical measurements) were too low by that factor compared to recent, more accurate cross sections deduced from electron-scattering measurements [19].

(b) At 30 eV the λ parameters of McAdams *et al.* [10], van Linden van den Heuvell, van Eck, and Heideman [17], and Steph and Golden [20] and the DCS's of Cartwright *et al.* [19] were utilized.

(c) At 40 eV the λ values were taken from Eminyan *et al.* [9] and Steph and Golden [20] and the DCS's from

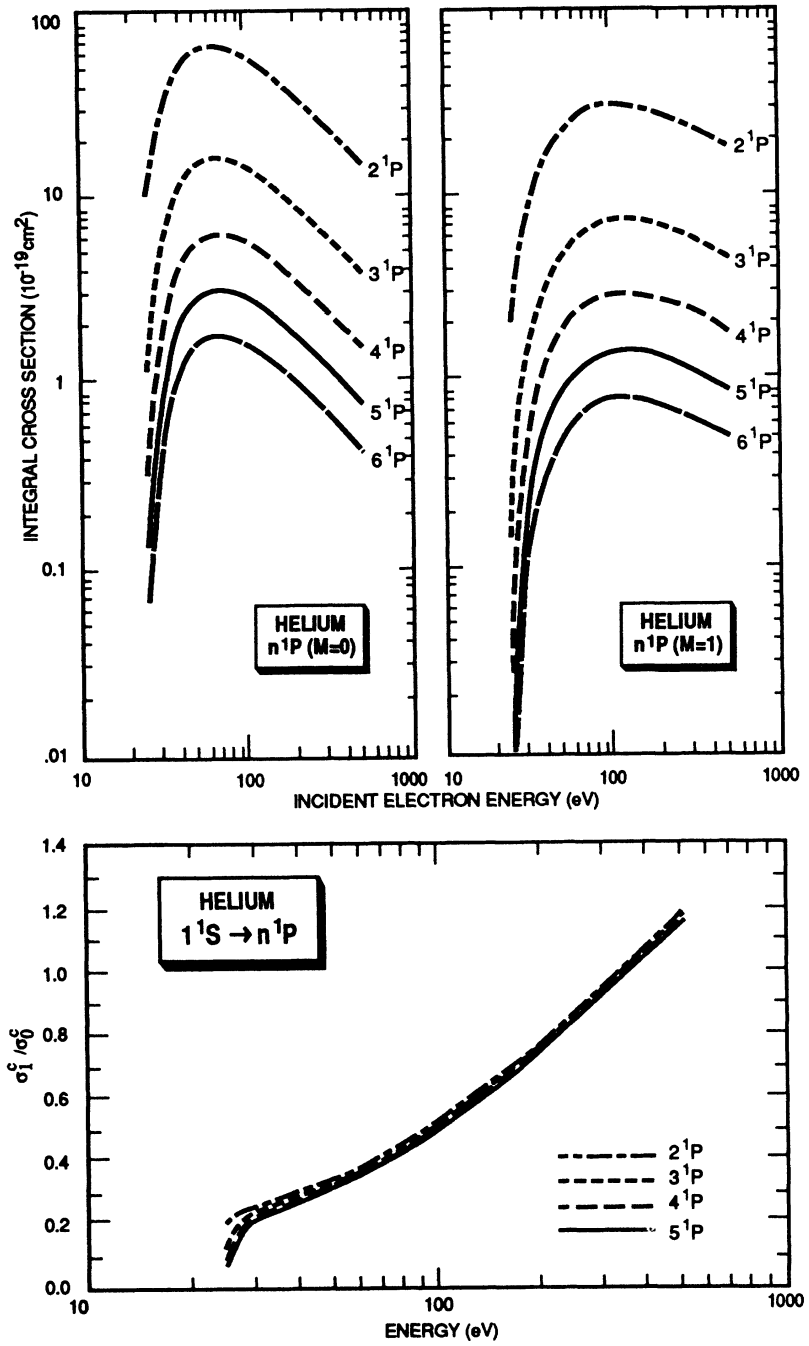

FIG. 17. (Upper two panels) Integral cross sections for excitation of the $M=0$ (left panel) and $|M=1|$ (right panel) magnetic sublevels in the $n\,^1P$ ($n=2,\ldots,6$) states. (Bottom panel) Ratio of the $|M=1|$ to $M=0$ integral cross section, as a function of the incident electron energy in the $n\,^1P$ ($n=2,\ldots,5$) states.

Hall *et al.* [21].

(d) At 50 eV we used λ parameters from Eminyan *et al.* [9], Tan *et al.* [11], and McAdams *et al.* [10] and DCS's from Cartwright *et al.* [19].

(e) At 60 and 80 eV Chutjian and Srivastava [5] reported collision DCS ($M=0$) utilizing their own DCS results and the λ parameters from Eminyan *et al.* [9]. We recalculated the collision DCS ($M=0$) using λ parameters from Eminyan *et al.* [9] and Slevin *et al.* [12] at 60 eV, and from Steph and Golden [13], Slevin *et al.* [12], Ugbabe *et al.* [14], and Eminyan *et al.* [9] at 80 eV. At both energies we utilized the $2\,^1P$ excitation to elastic-scattering intensity ratios of Chutjian and Srivastava [5] but recalculated the DCS values utilizing the recent elastic DCS data of Register *et al.* [15].

(f) At 100, 200, and 500 eV we used λ parameters reported by Eminyan *et al.* [9] and Steph and Golden [13]

TABLE IV. $n\,^1P$ magnetic-sublevel integral cross sections obtained from FOMBT calculations (10^{19} cm^2).

Energy	$2\,^1P$		$3\,^1P$		$4\,^1P$		$5\,^1P$		$6\,^1P$	
(eV)	$M=0$	$M=1$	$M=0$	$M=1$	$M=0$	$M=1$	$M=0$	$M=1$	$M=0$	$M=1$
25	10.20	2.041	1.157	0.1423	0.3270	0.02684	0.1357	0.008256	0.06898	0.003405
26.5	14.97	3.369	1.997	0.3630	0.6152	0.09576	0.2717	0.03884	0.1442	0.01928
27.5	18.29	4.299	2.663	0.5420	0.8467	0.1579	0.3805	0.06763	0.2031	0.03486
30	26.62	6.732	4.527	1.063	1.537	0.3485	0.7036	0.1561	0.3856	0.0846
35	41.15	11.33	8.271	2.168	3.012	0.7760	1.442	0.3673	0.8031	0.2039
40	51.50	15.19	11.23	3.162	4.227	1.173	2.065	0.5671	1.160	0.3173
50	62.21	20.84	14.92	4.832	5.695	1.793	2.812	0.8772	1.599	0.4963
60	65.41	24.48	15.91	5.689	6.266	2.206	3.105	1.087	1.770	0.6166
70	64.84	26.76	16.03	6.347	6.365	2.482	3.161	1.227	1.804	0.6964
80	62.62	28.17	15.65	6.764	6.234	2.659	3.109	1.317	1.775	0.7492
81.6	62.10	28.31	15.55	6.817	6.194	2.677	3.094	1.328	1.767	0.7562
100	56.84	29.4	14.34	7.172	5.741	2.834	2.866	1.408	1.638	0.8022
150	43.78	28.78	11.14	7.145	4.470	2.842	2.238	1.417	1.279	0.8083
200	34.98	26.82	8.910	6.705	3.575	2.672	1.789	1.334	1.023	0.7615
300	24.68	23.02	6.282	5.789	2.520	2.312	1.261	1.155	0.7213	0.6598
400	18.90	20.09	4.813	5.062	1.931	2.023	0.9661	1.011	0.5527	0.5777
500	15.16	17.86	3.870	4.502	1.553	1.800	0.7776	0.8999	0.4449	0.5143

and DCS's from Cartwright *et al.* [19] at 100 eV and from Dillon and Lassettre [23] at 200 and 500 eV.

In addition, at 50-, 60-, and 80-eV incident electron energies, Beijers *et al.* [22] reported P_l and γ values [35] in the 25°–100° angular range. We calculated the λ-values corresponding to their data [35] and used them in making our plots. In general these λ values are in agreement with the other λ values, but there are significant deviations at 50 eV in the 60°–70° range and at 90°, and at 60 eV in the 50°–70° range and at 100°.

C. Excitation of the $3\,^1P$ level

The procedure used in the case of the $2\,^1P$ level was also used to determine the $3\,^1P$ magnetic-sublevel DCS's. The results are summarized in Table III and compared with other results in Figs. 11–14.

(a) At 50 eV we used the DCS values of Cartwright *et al.* [19]. The λ values in the 10°–30° angular range were available from Eminyan *et al.* [24]. The λ values obtained by Crowe, King, and Williams [36] at 45.6-eV energy are in good agreement with those of Eminyan *et al.* [24] at angles below 20° but differ substantially in the 20°–30° range. van Linden van den Heuvell *et al.* [37] reported λ values in the 28–46-eV energy range but only at 35° scattering angle. An extrapolation of their results to 50-eV energy yields a λ value that is in good agreement with the value reported by Crowe, King, and Williams [36] at 45.6-eV incident electron energy at this angle. Beijers *et al.* [22] reported P_l and γ values [35] at 50-eV incident electron energy, in the 25°–85° scattered electron angular range from which we have calculated the corresponding λ values. These values are in good agreement with the results of Crowe, King, and Williams [36] and allowed us to extend the magnetic-sublevel DCS data to 85° scattering angle.

(b) At 80-eV incident electron energy, we recalculated

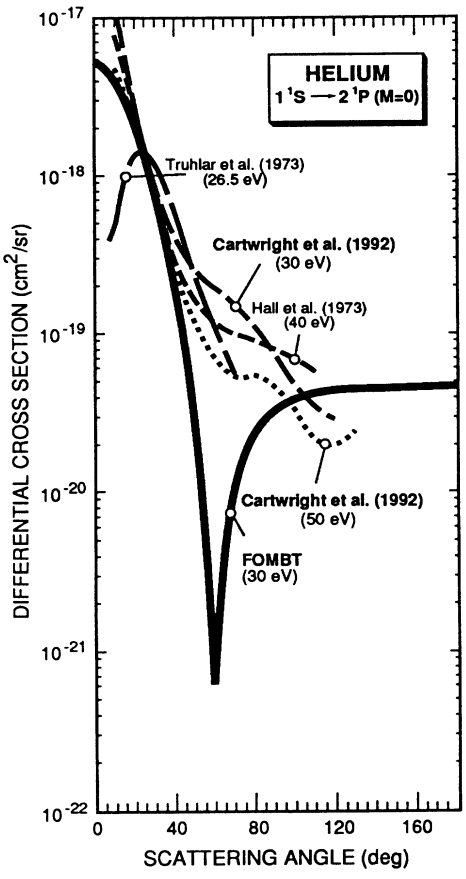

FIG. 18. Comparison of the FOMBT results (heavy line) at $E=30$ eV energy for the $2\,^1P$ excitation DCS ($M=0$) with experimental results in the 26.5 eV $\leq E \leq$ 50 eV energy range. The experimental results for the DCS used are those of Truhlar *et al.* [16], Cartwright *et al.* [19], and Hall *et al.* [21].

the DCS results of Chutjian [6] using his elastic to $3\,^1P$ excitation DCS ratios and the elastic scattering DCS values reported by Register, Trajmar, and Srivastava [15]. In the 5°–30° scattered electron angular range we used the λ values of Eminyan *et al.* [24]. Gelebart, Leguesdron, and Peresse [25] also reported a λ value at 80 eV but only at 10° scattering angle. This value is in excellent agreement with the value given by Eminyan *et al.* [24]. Crowe, King, and Williams [36] measured λ values at 75.6-eV incident electron energy that agree well with those of Eminyan *et al.* [24]. For the 60°–120° angular range, we used the λ parameters reported by McAdams and Williams [26] at 81.2-eV incident electron energy. We assumed that the λ and DCS values did not change with the energy over this small energy range. We also calculated λ values [35] from the P_l and γ values given by Beijers *et al.* [22] and found them to be in good agreement with those of Eminyan *et al.* [24] at low angles and with those of McAdams and Williams [26] at high angles (except for 45° and 65° scattering angles). At 100-eV incident electron energy, the DCS data were taken from Cartwright *et al.* [19] and the λ values from Eminyan *et al.* [24].

The DCS ($M=0$) results at 70-eV incident electron energy are from Hummer and Burns [7]. They obtained relative DCS ($M=0$) values from EPC experiments and we normalized their relative data at 10° scattering angle to our FOMBT result.

III. COMPARATIVE THEORETICAL STUDIES

In order to get more physical insight into magnetic-sublevel excitation cross sections, we also studied the behavior of our theoretical results as a function of incident electron energy and principal quantum number of the final state (see Figs. 15–17). In Fig. 15 we show the energy dependence of the DCS ($M=0$) for the $n\,^1P$ ($n=2,\ldots,5$) excitations, and in Fig. 16 we show the principal quantum number dependence (for $n=2$–5) of the DCS ($M=0$) angular distributions for selected energies in the 25 eV $\leq E \leq$ 81.6 eV energy range. In Table IV we give our FOMBT results for the $n\,^1P$ ($n=2,3,4,5$) excitation magnetic sublevel integral cross sections and Fig. 17 shows the energy dependence of σ_0^c and σ_1^c for the $n\,^1P$ ($n=2,3,\ldots,6$) excitations as well as the σ_1^c/σ_0^c ratio for $n\,^1P$ ($n=2,\ldots,5$) excitations as a function of incident electron energy.

IV. DISCUSSION

It is interesting that for both the $2\,^1P$ and $3\,^1P$ excitation processes at all energies studied, the magnetic-sublevel cross sections are generally predicted correctly by FOMBT for both magnitude and shape. A major exception appears to be the strong minimum predicted by FOMBT for the $2\,^1P$ excitation DCS ($M=0$) for incident energies about 30 eV. As is shown in Fig. 18, the "experimental" DCS ($M=0$) for $2\,^1P$ excitation does not appear to display the sharp minimum predicted by FOMBT at $E=30$ eV energy. As is shown in Fig. 19, this strong minimum is the result of the FOMBT result for λ at and around $E=30$ eV, which disagrees with all experimental data for λ at this energy. This seems to be a defect in FOMBT for $M=0$ at this energy that does not appear in the DCS (summed over M) predicted by FOMBT (see right panel in Fig. 3). It is interesting to note, however, that the DCS ($M=0$) deduced at 25.6 eV appears to be dropping to a minimum. It is also interesting to note, as shown in Fig. 15, that this minimum predicted by FOMBT is deepest at $E=30$ eV and the sharp minimum quickly disappears at higher energies; however, a "shoulder" in the DCS ($M=0$) is still discernible even at $E=100$ eV incident electron energy and this characteristic is also present for the $3\,^1P$ excitation. FOMBT is not

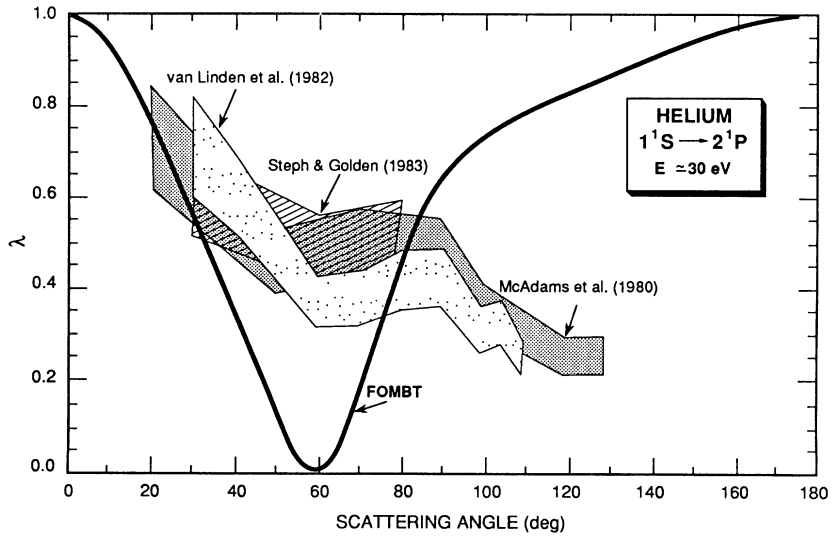

FIG. 19. Comparison of FOMBT results at $E=30$ eV energy for the $2\,^1P$ excitation λ EICP with experimental results in the 29.6 eV $\leq E \leq$ 30 eV energy range. Experimental results shown are those of van Linden van den Huevell, van Eck, and Heideman [17], Steph and Golden [20], and McAdams *et al.* [10].

expected to give excellent results for energies as low as $E=30$ eV (~ 10 eV above threshold) where higher-order effects can be important. It would be interesting to see whether close-coupling or R-matrix theory results show the strong minimum at 30 eV. The most notable deviations of FOMBT predictions from experiment are the predictions of the minimum in the DCS ($M=0$) for 25 eV $\leq E \leq 80$ eV (see Fig. 15) and the somewhat faster drop of the FOMBT results through the experiment in the DCS ($M=1$) for the same energy range. The reason for this behavior is not known to us. One should also remember that the accuracy of the experimental data for λ decreases with increasing angle. In spite of these deviations, it is remarkable how well FOMBT describes the magnetic sublevel excitation DCS's for all energies studied. Both of these deviations disappear simultaneously for about $E=81.6$ eV incident electron energy, and for $E \geq 100$ eV there is practically perfect agreement between theory and experiment for the magnetic sublevel DCS's.

We show in Fig. 16 the n dependence for $n=2-5$ of the DCS ($M=0$). Based on our earlier analysis of the n dependence of DCS's and EICP's, we expect the n dependent magnetic sublevel DCS's to be practically identical in shape and differ only by a scale factor. This behavior is conspicuous for $E=40$ and 81.6 eV energies (see Fig. 16), but it is missing at $E=25$ eV incident electron energy and is not perfect for $E=30$ eV energy. As we stated earlier, the simple n dependence of the DCS's is expected only at the higher energies and that is exactly what we found here. The energy dependence of the σ_1^c and σ_0^c magnetic sublevel integral cross sections for $n\,^1P$ ($n=2,3,\ldots,6$) excitation is practically identical, showing again a simple scaling relationship among them, discussed in the previous paper [14]. The σ_1^c/σ_0^c ratio shown in Fig. 17 for $n\,^1P$ ($n=2,\ldots,5$) excitations as a function of energy appears to be practically independent of the principal quantum number n. This has been already observed in conjunction with the n independence of the polarization fractions for a wide range of energies [38]. These latter results indicate that for the small scattering angles, that contribute most significantly to the ICS's, the scaling relationship is more exact than for large angles. It would be interesting to see whether these predictions, based on the FOMBT results, can be confirmed experimentally.

ACKNOWLEDGMENTS

David C. Cartwright and George Csanak gratefully acknowledge the financial support of the U.S. DOE, the NSF (OIP), and the University of California (Riverside)—Los Alamos National Laboratory Collaborative Research Program (CALCOR) for this study. Partial support for S.T. JPL, Caltech by NASA is acknowledged.

[1] M. Eminyan, K. B. McAdam, J. Slevin, and H. Kleinpoppen, Phys. Rev. Lett. **31**, 576 (1973); J. Phys. B **7**, 1519 (1974).
[2] K. Blum and H. Kleinpoppen, Phys. Rep. **52**, 203 (1979); Adv. At. Mol. Phys. **19**, 187 (1983).
[3] N. Anderson, J. W. Gallagher, and I. V. Hertel, Phys. Rep. **165**, 1 (1988).
[4] J. A. Slevin and S. Chwirot, J. Phys. B **23**, 165 (1990).
[5] A. Chutjian and S. K. Srivastava, J. Phys. B **8**, 2360 (1975).
[6] A. Chutjian, J. Phys. B **9**, 1749 (1976).
[7] C. R. Hummer and D. J. Burns, Phys. Rev. A **33**, 2995 (1986).
[8] G. Csanak, H. S. Taylor, and R. Yaris, Phys. Rev. A **3**, 1322 (1971).
[9] M. Eminyan, K. B. McAdam, J. Slevin, M. C. Standage, and H. Kleinpoppen, J. Phys. B **7**, 1519 (1974).
[10] R. McAdams, M. T. Hollywood, A. Crowe, and J. F. Williams, J. Phys. B **13**, 3691 (1980).
[11] K. H. Tan, J. Fryar, P. S. Farago, and J. W. McConkey, J. Phys. B **10**, 1073 (1977).
[12] J. Slevin, H. Q. Porter, M. Eminyan, A. Defrance, and G. Vassilev, J. Phys. B **13**, 3009 (1980).
[13] N. C. Steph and D. E. Golden, Phys. Rev. A **21**, 1984 (1980).
[14] A. Ugbabe, P. J. O. Teubner, E. Weigold, and H. Arriola, J. Phys. B **10**, 71 (1977).
[15] D. F. Register, S. Trajmar, and S. K. Srivastava, Phys. Rev. A **21**, 1134 (1980).
[16] D. G. Truhlar, J. K. Rice, A. Kuppermann, S. Trajmar, and D. C. Cartwright, Phys. Rev. A **1**, 778 (1970).
[17] H. B. van Linden van den Heuvell, J. van Eck, and H. G. M. Heideman, J. Phys. B **15**, 3517 (1982).
[18] A. Crowe and J. C. Nogueira, J. Phys. B **15**, L501 (1982).
[19] D. C. Cartwright, G. Csanak, S. Trajmar, and D. C. Register, preceding paper, Phys. Rev. A **45**, 1602 (1992).
[20] N. C. Steph and D. E. Golden, Phys. Rev. A **27**, 1678 (1983).
[21] R. I. Hall, G. Joyez, Y. Mazeau, J. Reinhardt, and C. Schermann, J. Phys. (Paris) **34**, 827 (1973).
[22] J. P. M. Beijers, D. H. Madison, J. van Eck, and H. G. M. Heideman, J. Phys. B **20**, 167 (1987).
[23] M. A. Dillon and E. N. Lassettre, J. Chem. Phys. **63**, 2373 (1975).
[24] M. Eminyan, K. B. McAdam, J. Slevin, M. C. Standage, and H. Kleinpoppen, J. Phys. B **8**, 2058 (1975).
[25] G. Gelabert, H. Leguesdron, and J. Peresse, Phys. Lett. **87A**, 345 (1982).
[26] R. McAdams and J. F. Williams, J. Phys. B **15**, L247 (1982).
[27] M. J. Brunger, I. E. McCarthy, K. Ratnavelu, P. J. O. Teubner, A. M. Weigold, Y. Zhou, and L. J. Allen, J. Phys. B **22**, 1325 (1990).
[28] D. H. Madison, J. Phys. B **12**, 3399 (1979); D. H. Madison and K. H. Winters, *ibid.* **16**, 4437 (1983); K. Bartschat and D. H. Madison, *ibid.* **8**, 153 (1988); and private communication from D. H. Madison (unpublished).
[29] K. Bhadra, J. Callaway, and R. J. W. Henry, Phys. Rev. A **19**, 1841 (1979).
[30] L. D. Thomas, B. S. Yarlagadda, H. S. Taylor, and G. Csanak, J. Phys. B **7**, 1719 (1974).
[31] W. C. Fon, K. A. Berrington, and A. E. Kingston, J. Phys. B **13**, 2309 (1980).
[32] T. Scott and M. R. C. McDowell, J. Phys. B **8**, 2369

(1975).
[33] M. R. Flannery and K. J. McCann, J. Phys. B **8**, 1716 (1975).
[34] J. D. Jobe and R. M. St. John, Phys. Rev. **164**, 117 (1967).
[35] For the definition of the γ and P_l parameters, see Refs. [3] and [24]. λ can be obtained from γ and P_l via the simple formula $\lambda=(I+P_l\cos 2\gamma)/2$.
[36] A. Crowe, T. C. F. King, and J. F. Williams, J. Phys. B **14**, 1219 (1981).
[37] H. B. van Linden van den Heuvell, E. M. van Gasteren, J. van Eck, and H. G. M. Heideman, J. Phys. B **16**, 1619 (1983).
[38] G. Csanak and D. C. Cartwright, J. Phys. B **22**, 2769 (1989).

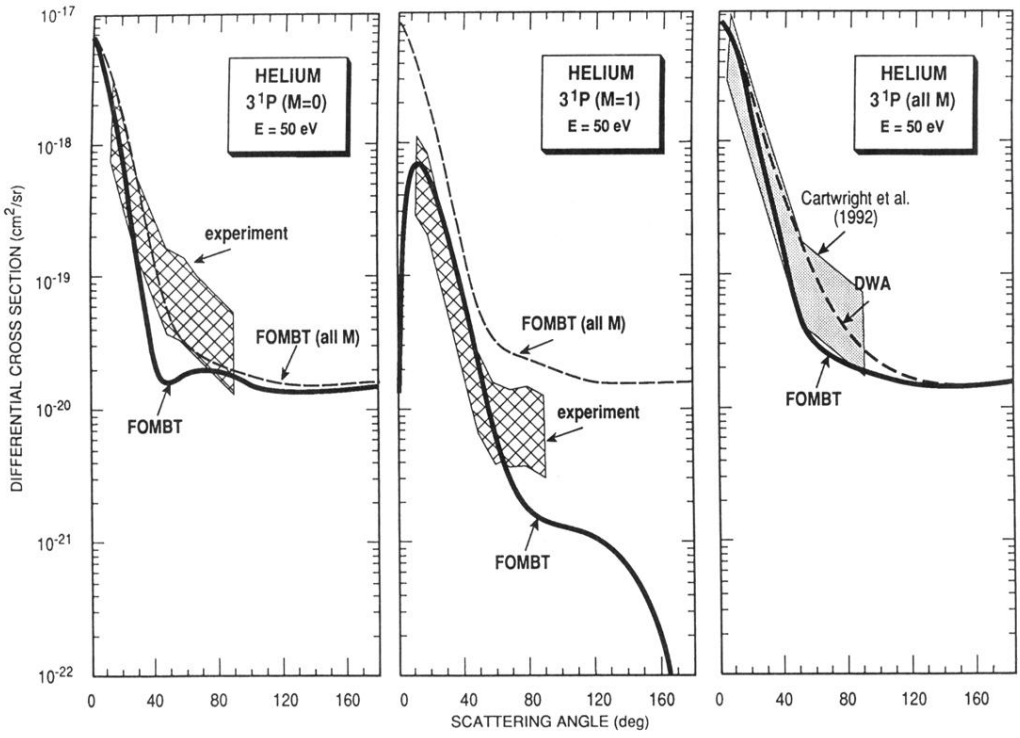

FIG. 11. Same as Fig. 2 except for magnetic-sublevel DCS's (left two panels) and magnetic-sublevel summed DCS (right panel) for the electron-impact excitation of the $3\,^1P$ state of helium at $E=50$ eV incident electron energy. The experimental DCS data used (shown in the right panel) are from Cartwright *et al.* [19]. As with the previous figures, the summed magnetic-sublevel DCS has been included in the left and center panels as the dashed curve to enable comparison with the magnetic-sublevel DCS.

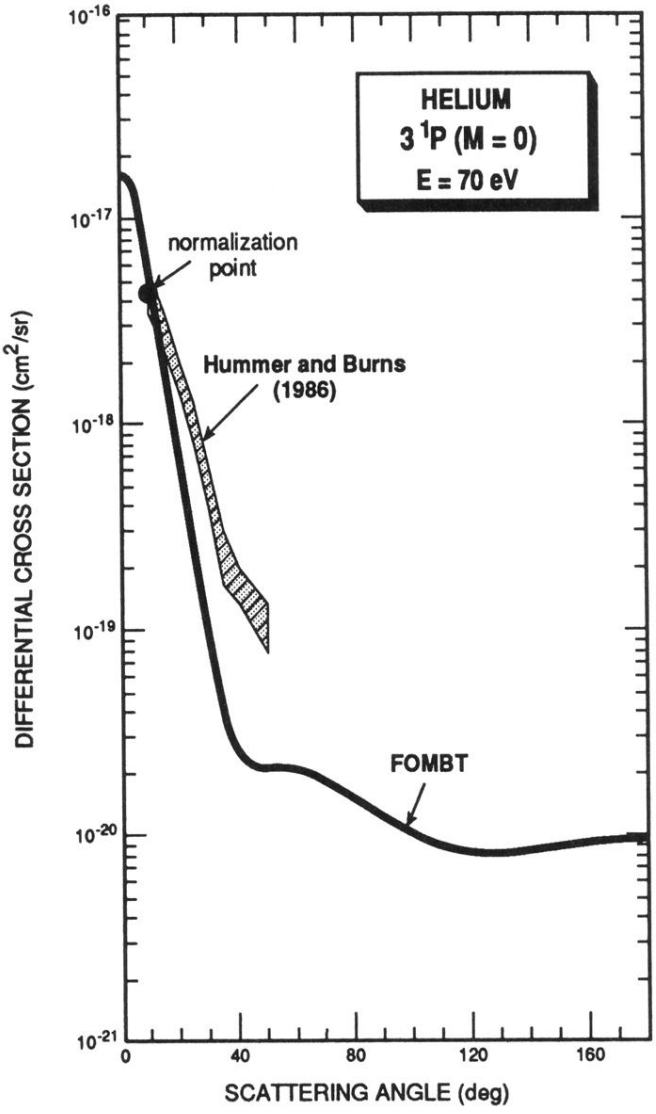

FIG. 12. Comparison of FOMBT results for the DCS ($M=0$) with the experimental data of Hummer and Burns [7] for $E=70$ eV incident electron energy. The relative experimental DCS ($M=0$) results were normalized to our FOMBT results at the smallest experimental scattering angle ($\theta=10°$).

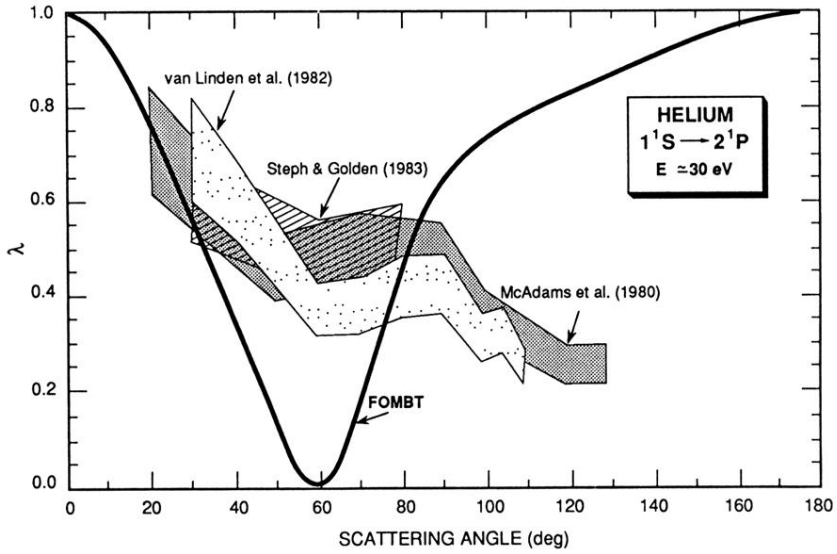

FIG. 19. Comparison of FOMBT results at $E = 30$ eV energy for the $2\,^1P$ excitation λ EICP with experimental results in the 29.6 eV $\leq E \leq$ 30 eV energy range. Experimental results shown are those of van Linden van den Huevell, van Eck, and Heideman [17], Steph and Golden [20], and McAdams *et al.* [10].

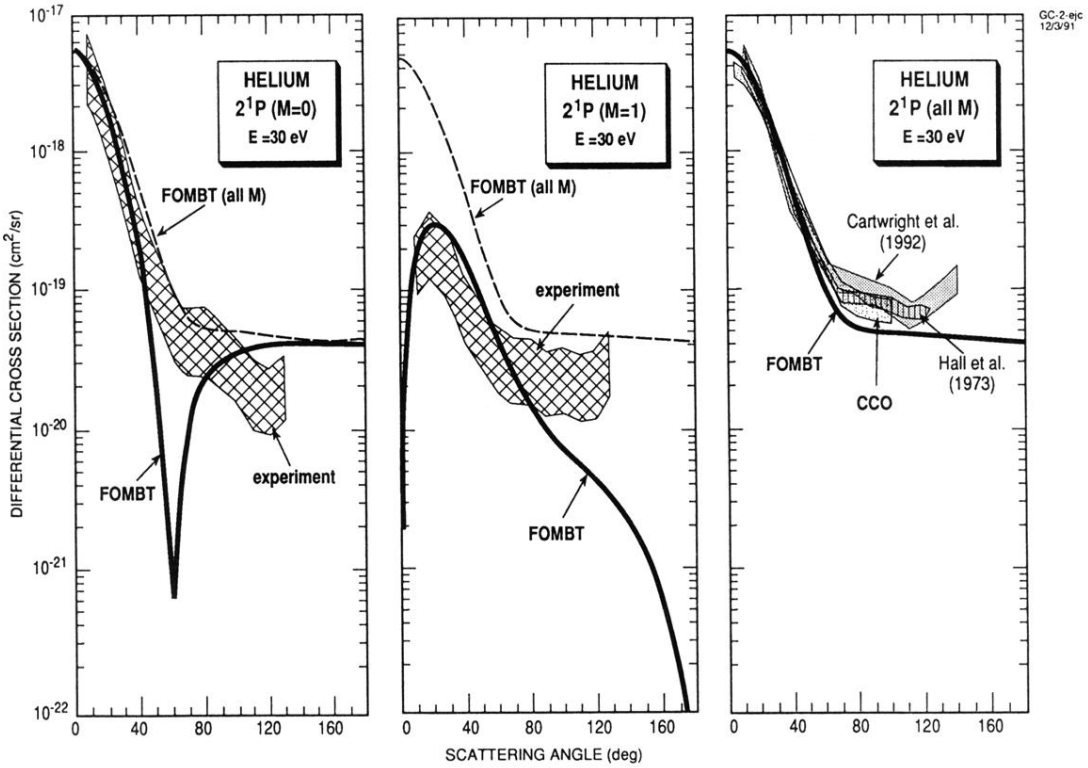

FIG. 3. Same as Fig. 2 except for $E = 30$ eV incident electron energy. The experimental DCS data used are from Cartwright *et al.* [19] and from Hall *et al.* [21] (shown in right panel). The ten-channel optical potential close-coupling (CCO) results of Brunger *et al.* [27] for the DCS are also shown.

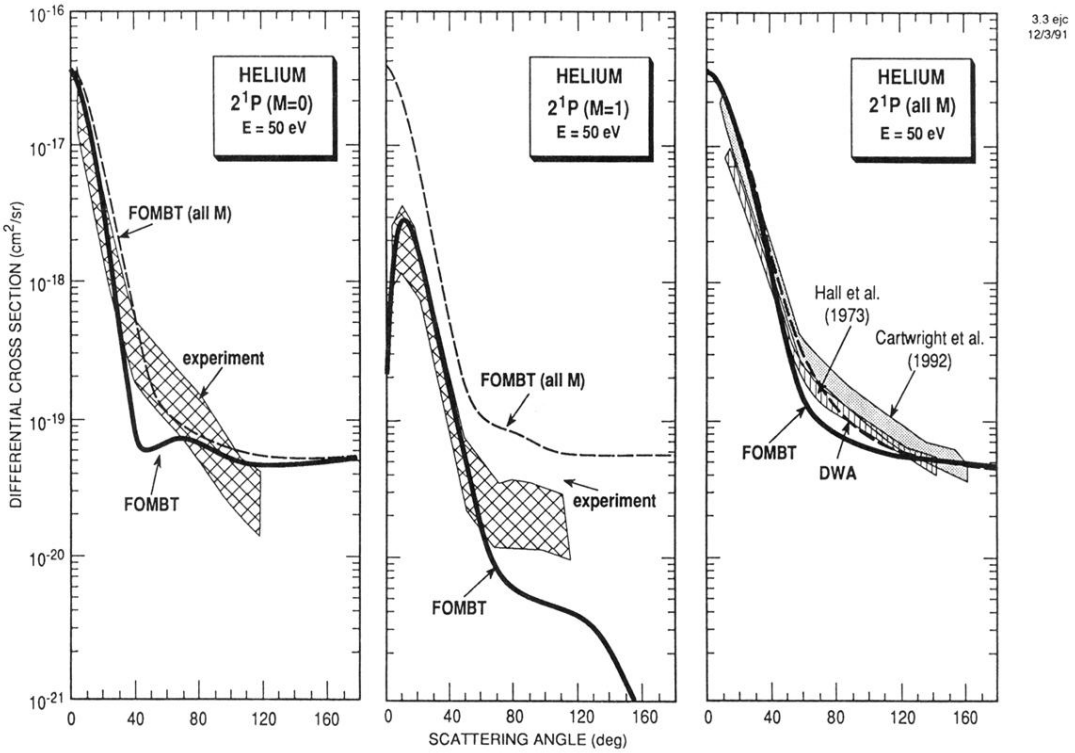

FIG. 5. Same as Fig. 3 except for $E = 50$ eV incident electron energy. The experimental DCS data used are from Hall *et al.* [21] and from Cartwright *et al.* [19] (shown in the right panel). The DWA results of Madison and co-workers [28] are also shown in the right panel for comparison.

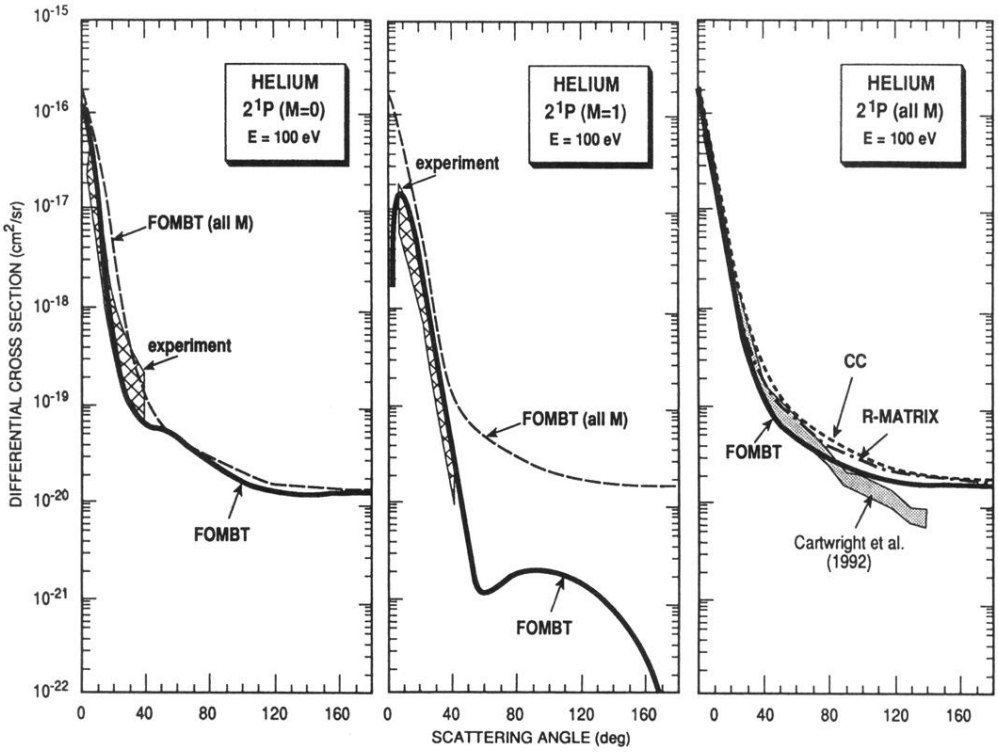

FIG. 8. Same as Fig. 2 except for $E = 100$ eV incident electron energy. The experimental DCS data used are from Cartwright *et al.* [19] (shown in the right panel). The five-state CC results of Bhadra, Callaway, and Henry [29] and the five-state R-matrix (R-MATRIX) results of Fon, Berrington, and Kingston [31] are also shown.